A FLAT HIGH-FREQUENCY SCANNING MICROMIRROR

Robert A. Conant, Jocelyn T. Nee, Kam Y. Lau, and Richard S. Muller
Berkeley Sensor & Actuator Center, University of California, Berkeley
Berkeley, CA 94720-1774

ABSTRACT

We present the Staggered Torsional Electrostatic Combdrive (STEC) fabrication process that creates thick mirrors with high-torque actuators, thereby allowing high-speed optical scanning with large angular deflections. We have demonstrated a 550 µm-diameter mirror capable of scanning an optical angle of 24.9° at its 34 kHz resonant frequency with less than 30 nm static and dynamic deformation. The optical resolution is 350 pixels – very near the diffraction-limited resolution of 355 pixels with 655 nm wavelength light.

INTRODUCTION

Scanning mirrors are used in many applications: barcode readers, laser printers, confocal microscopes, and fiber-optic network components. There are significant limitations to the performance of macro-scale scanners; in particular, their scanning speed, power consumption, cost, and size often preclude their use in portable systems. In addition, higher-frequency optical scanning could enable new applications that are not practical with conventional scanning mirrors, such as raster-scanning projection video displays [1], and would significantly improve the performance of scanning mirrors in existing applications, such as laser printers. MEMS optical scanners promise to enable these new applications, and dramatically reduce the cost of optical systems.

However, previously demonstrated MEMS mirrors have not been able to simultaneously meet the requirements of high scan speed *and* high resolution. A plethora of micromirror designs have been presented, but none has been able to satisfy the potential of MEMS: a high-speed, high-performance scanning mirror. For example, surface-micromachined scanning mirrors actuated with electrostatic combdrives have been shown to operate at high scan speeds (up to 21 kHz), but static and dynamic mirror deformation limits the resolution to less than 20% of the diffraction-limited resolution. Magnetically actuated mirrors have been demonstrated with high speed and large amplitude [2], but have not demonstrated high resolution, and often require off-chip actuation.

In order to take advantage of the unique capabilities of micromachining technology, we have fabricated a new type of micromirror capable of high-speed, high-resolution scanning with low power consumption.

THEORY OF OPERATION

STEC Micromirror

Figure 1 shows a schematic of the Staggered Torsional Electrostatic Combdrive (STEC) micromirror, which is made from two layers of single-crystal silicon separated by a 1.7 µm-thick silicon dioxide layer. The mirror, torsion hinge, and moving comb teeth are in the top silicon layer, and the fixed comb teeth are in the bottom silicon layer. Applying voltage between the top and the bottom layers attracts the moving comb teeth to the fixed comb teeth, thus exerting torque on the mirror and causing it to tilt. The torsion hinges, which are anchored to the bottom silicon layer, provide restoring torque. Similar torsional actuators have been
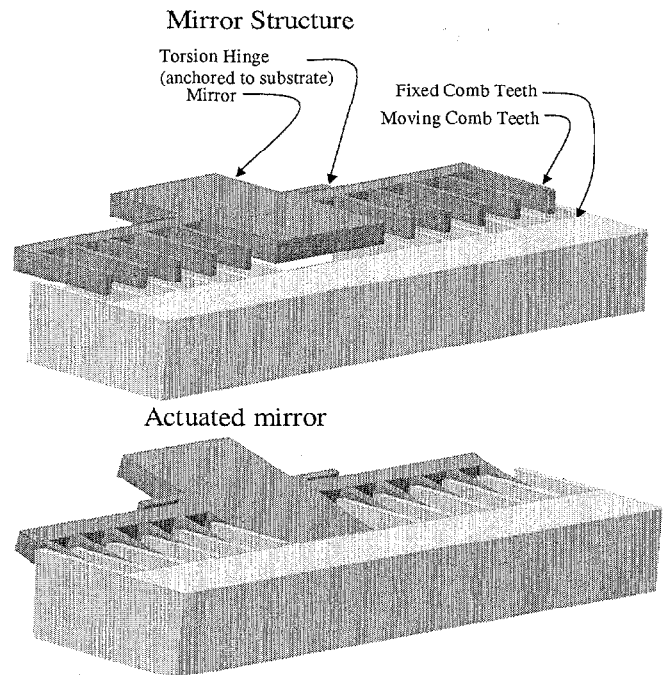
Mirror Structure

Actuated mirror

Figure 1. Schematic of a STEC micromirror. Applying a voltage between the top and the bottom layers generates a torque on the mirror, thereby causing it to tilt.

described earlier [3][4]. SEMs of the completed STEC micromirror are shown in Figure 2.

This torsional electrostatic combdrive offers several advantages over other electrostatic-actuator designs. First, the actuator applies torque to the mirror directly – there are no hinges to couple linear motion of an actuator into torsional mirror motion. This greatly simplifies the design of the structure, and makes post-fabrication assembly steps unnecessary.

Second, the actuator starts in an unbalanced state and is capable of static mirror positioning as well as resonant scanning. Previously demonstrated balanced torsional electrostatic actuators have been very promising for resonant operation [5], but are not capable of static mirror positioning.

Third, the torsional combdrive offers an advantage over gap-closing actuators because the energy density in the combdrive is higher than that in a gap-closing actuator, thereby allowing larger scan angles at high resonant frequencies.

Optical Resolution

The optical resolution – defined as the ratio of the optical-beam divergence and the mirror scan angle – is an essential performance metric for a scanning mirror. For a perfectly flat mirror under uniform illumination, the farfield intensity distribution is an Airy pattern, which has a full-width-half-max half-angle beam divergence α (the resolution criteria used for video displays [6]) given by
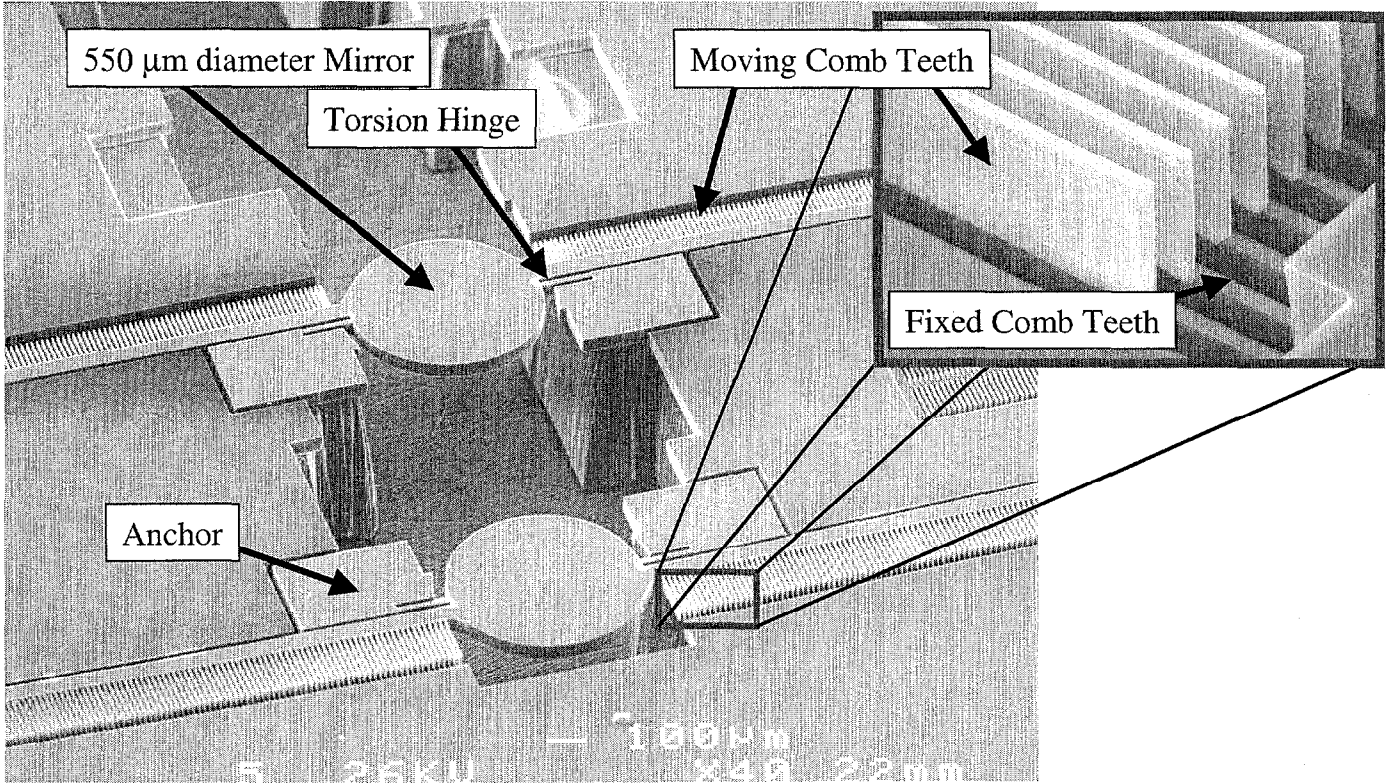
$$\alpha = \frac{1.03\lambda}{D} \qquad [1]$$

Figure 2. SEM of two STEC micromirrors. The SEM chuck is visible through the wafer below the mirror. The inset SEM in the upper right shows a close-up view of the fixed and moving combteeth.

where λ is the wavelength of the incident light, and D is the mirror diameter. The resulting optical resolution N is

$$N = \frac{4\theta}{\alpha} = \frac{4\theta D}{1.03\lambda} \qquad [2]$$

where θ is the mechanical half-angle mirror scan (the total optical scan is 4θ).

Dynamic mirror deformation can also contribute to beam divergence, thereby decreasing the optical resolution. For a mirror where the torsion hinge is the dominant compliance, the nonplanar surface deformation δ of a rectangular scanning mirror of half-length L with angular acceleration $(2\pi f)^2 \theta$ (where f is the scan frequency) is [7]

$$\delta = 0.183 \frac{\rho(1 - v^2)(2\pi f)^2 \theta}{Et^2} L^5 \qquad [3]$$

where ρ is the material density, v is Poisson's ratio, E is Young's modulus, and t is the mirror thickness.

The Rayleigh limit, the maximum amount of surface deformation tolerable without significant degradation in image quality, allows a peak-to-valley surface deformation of $\lambda/4$ [8]. For a 550 μm-long (275 μm-half-length) rectangular single-crystal-silicon mirror of thickness 50 μm, half-angle mechanical scan 6.25°, and resonant frequency 34 kHz, the calculated dynamic deformation is 8 nm – much lower than the Rayleigh limit for 655 nm light (164 nm). For comparison, a 550 μm-long surface-micromachined mirror of thickness 1.5 μm maintains the surface flatness within the Rayleigh limit only up to a frequency of 4.6 kHz.

FABRICATION

The STEC micromirrors are fabricated using deep reactive-ion etching and a bond-and-etchback process with a buried pattern. The process flow is shown in Figure 3.

First, a silicon wafer is oxidized in steam at 1000°C to grow 0.2 μm of thermal oxide. This wafer is patterned with the BURIED pattern, and 100 μm-deep trenches are etched into the wafer using an STS deep reactive-ion etcher to form the fixed combteeth. This wafer, along with another wafer having 1.5 μm of thermal oxide, is cleaned and the two wafers are bonded together with the fixed combteeth at the wafer interface. The bonded wafer pair is then annealed at 1100°C for one hour to increase the bond strength [9].

Next, the bonded wafer is ground and polished to leave a 50 μm-thick layer of silicon above the oxide interface. The resulting silicon-on-insulator (SOI) wafer is oxidized at 1100°C in a steam ambient to form a 1.1 μm-thick oxide layer on the top and bottom. Alignment between the subsequent patterns and the buried combteeth is achieved by etching a window in the top-layer silicon above the two dice used to align the mask to the wafer. These two dice are sacrificed to achieve the necessary alignment precision between the moving combteeth (on the top layer) and the fixed combteeth (on the bottom layer).

The FRONTSIDE pattern, which defines the moving comb teeth, the mirror, and the torsion hinges, is then patterned and etched into the top oxide layer (the pattern is etched into the silicon in a later step). The alignment of this step is critical because misalignment between the moving combteeth and the fixed combteeth can lead to instability in the torsional combdrive. We have typically been able to achieve better than 0.2 μm alignment between the BURIED pattern and the FRONTSIDE
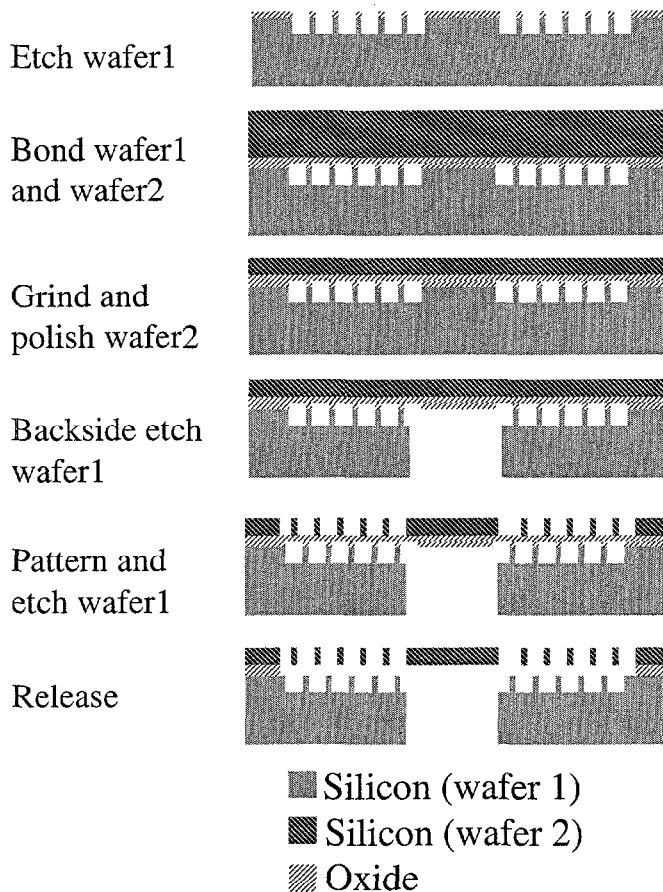
Etch wafer1

Bond wafer1
and wafer2

Grind and
polish wafer2

Backside etch
wafer1

Pattern and
etch wafer1

Release

▓ Silicon (wafer 1)
▓ Silicon (wafer 2)
▓ Oxide

Figure 3. STEC micromirror fabrication process flow.

pattern using a GCA i-line wafer stepper, and this alignment error has not limited the STEC micromirror performance.

Next, the oxide and silicon on the backside of the bottom wafer are patterned with the HOLE layer, and the entire bottom wafer is etched to open an optical path underneath the micromirror. The silicon on the top layer is then etched using the previously patterned top oxide layer as an etch mask. The structure is released with a timed HF etch to remove the sacrificial oxide film below the combteeth and mirror. Finally, a 100 nm-thick aluminum film is evaporated onto the bottom of the mirror to increase the reflectivity for visible light to approximately 92% [10].

RESULTS

The STEC mirror excels in all of the critical performance criteria: cost, resolution, scan speed, scan repeatability, size, power consumption, and reliability. This section discusses measurements of four of these performance criteria for one STEC mirror design.

Resolution

The surface deformation of the micromirror was characterized using the stroboscopic interferometer reported in [11]. Figure 4 shows the dynamic deformation of the micromirror at the end of the scan where the dynamic deformation reaches its maximum. The total deformation is less than 30 nm, considerably below the Rayleigh limit, and does not significantly reduce the optical resolution.

Figure 5 shows a photograph of the scan of a STEC mirror with a 655 nm laser pulsed synchronously with the mirror scan to generate 43 spots. The mirror scan is sinusoidal, so the timing of

the laser pulses was adjusted across the scan to produce equally spaced spots. Figure 5 also shows a close-up image of three individual spots captured with a CCD camera. By fitting a Gaussian curve to each of these three spots, we were able to determine the full-width-half-max beam width and the distance between the spots. The spot size and separation at eight different regions across the scan give the measured total optical resolution of 350 pixels. The resolution of this 550 μm-diameter mirror with 24.9° optical scan and 655 nm laser light is near the diffraction-limited resolution of 355 pixels from Eq. [2].

Scan Speed

STEC micromirrors have been demonstrated with diameters of 550 μm and resonant frequencies up to 42 kHz – almost an order of magnitude faster than commercially available optical scanners. Larger STEC mirrors have also been fabricated (up to 2 mm) with lower resonant frequencies. Figure 6 shows the frequency response of a 550 μm-diameter micromirror.

The main limitation of macro-scale scanners comes from the dynamic deformation described by Eq.[3] – the dynamic deformation scales as the fifth power of the mirror length, so large mirrors scanning at high speeds will have considerable dynamic deformation. For example, a 10 mm-diameter, 1 mm-thick mirror with a mechanical scan of ±6.25° maintains less than 164 nm dynamic deformation (the Rayleigh limit for 655 nm light) up to a frequency of only 2.2 kHz. Large-scale mirrors cannot achieve the speeds demonstrated with the STEC micromirrors without severe dynamic deformation or very thick mirrors.

Power Consumption

High-speed scanners require more torque than low-speed scanners to reach the same scan angle. In order to generate the torque necessary for large angle, high-frequency operation of the STEC micromirror, we use fairly high voltages. The 550 μm-diameter mirror with resonant frequency 34 kHz requires a 171 Vrms input sine wave for a total optical scan of 24.9°. To simplify mirror testing and operation, we use a small (1 cm^3) 25:1 transformer, allowing us to use a conventional 0-10 V function generator to drive the scanning mirrors with a sinusoidal waveform of amplitude up to 250 V. The use of the transformer also provides efficient power conversion, so the power consumption of the entire system can be much lower than systems requiring high-voltage power supplies and opamps.

This power consumption is the sum of the power dissipation in the drive electronics and the power dissipated by air and material damping. The power consumption due to damping is

$$P = \frac{1}{2}b\theta^2\omega^2 = \frac{1}{2}\frac{k}{Q}\theta^2\omega \qquad [4]$$

where k is the torsional spring stiffness, b is the torque damping factor, θ is the mechanical scan half angle (the total optical scan is $\pm 2\theta_0$), ω is the resonant frequency, and Q is the resonant quality factor. For the 34 kHz 550 μm-diameter mirror scanning 25° optical (±6.25° mechanical), the calculated stiffness $k = 3.93 \times 10^{-5}$ Nm/radian, the measured resonant quality factor $Q = 273$, so the power consumption due to damping from Eq. [4] is 0.18 mW. Vacuum packaging can be used to reduce the viscous damping, and thereby decrease the power consumption.

The measured power consumption is 6.8 mW, indicating that the majority of the power consumption is in charging and discharging the parasitic capacitance and losses in the transformer power conversion.
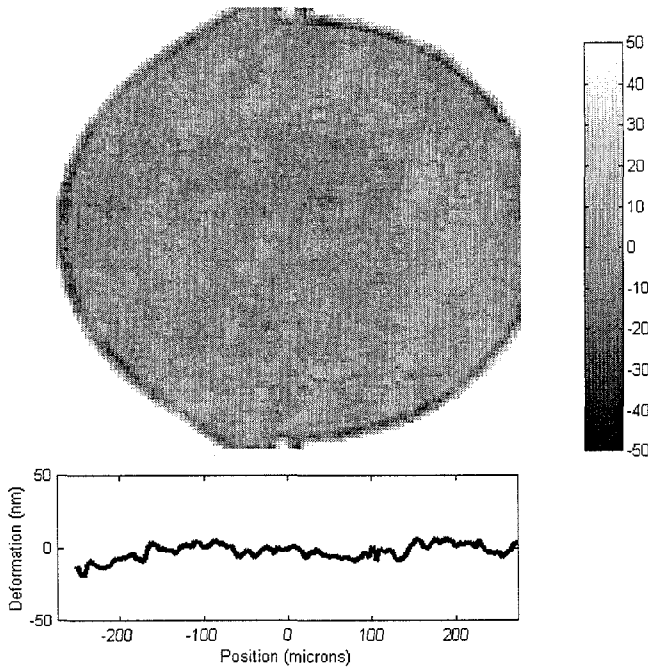
Figure 4. *Static and dynamic deformation of the 550 μm-diameter mirror is less than 30 nm. The graph below the grayscale surface height map shows the measured mirror deformation along the center of the mirror perpendicular to the torsion hinges.*

Reliability

The STEC micromirror is expected to be extremely reliable due to its simple structure. It is predicted that the failure point for the structure will be the torsion hinges (at the point of highest strain). The maximum strain in a 50 μm-thick, 15 μm-wide, 150 μm-long hinge (the hinge used for the 550 μm-diameter mirror with resonant frequency of 34 kHz) with a total scan of ±6.25° is approximately 1.8%. Mirrors have been operated at this level for over 200 million cycles without any noticeable degradation in performance, but this strain may be too high for acceptable long-term reliability. Future designs will use wider, longer hinges to reduce the maximum strain while retaining the same stiffness.
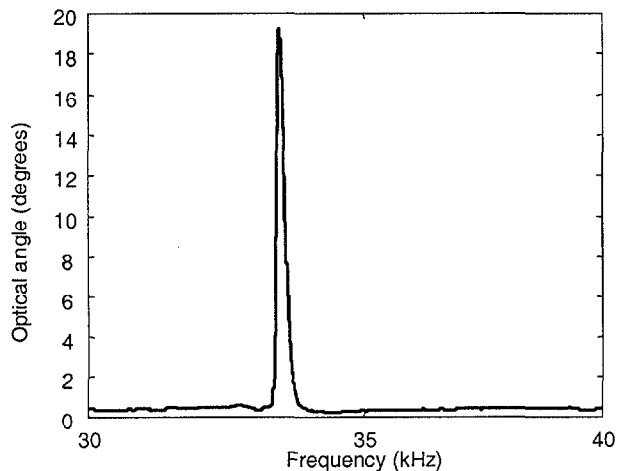

Figure 6: Frequency response of STEC micromirror.

CONCLUSIONS

The potential of micromachined mirrors over conventional scanning mirrors – high scan speed, small size, and low cost with diffraction-limited optical performance – has been demonstrated
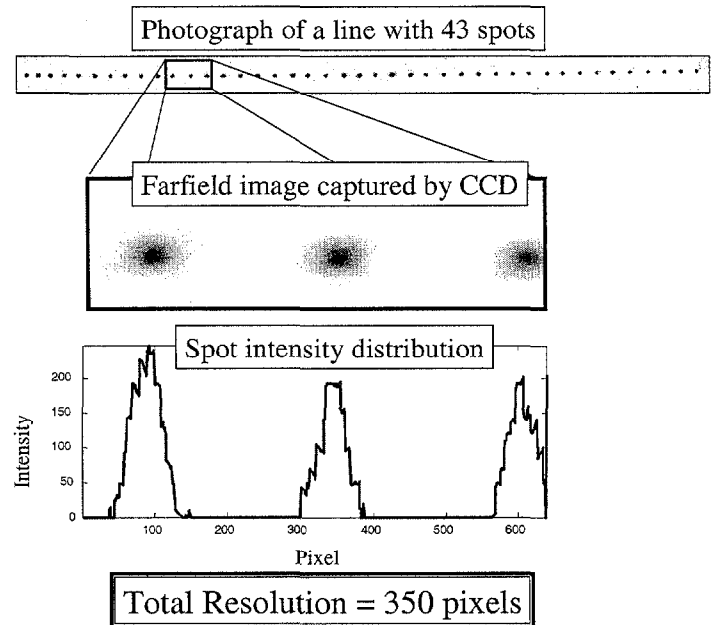

Figure 5. *Optical scan of STEC micromirror operating at 34 KHz, with close-up image of spots and intensity distribution plot. The images recorded on the photograph and the CCD, which were red-on-black, were converted to black-on-white for this figure.*

with the Staggered Torsional Electrostatic Combdrive (STEC) micromirror. The scan speed of the STEC micromirror is difficult to achieve with large-scale optical scanners, and exceeds the performance of previously demonstrated micromachined scanning mirrors.

REFERENCES

1. R.A. Conant, P.M. Hagelin, U. Krishnamoorthy, O. Solgaard, K.Y. Lau, R.S. Muller, "A Full-Motion Video Display Using Micromachined Scanning Micromirrors," proc. Transducers '99, Sendai, Japan (1999), pp. 376-379.
2. A. Garnier, T. Bourouina, H. Fujita, T. Hiramoto, E. Orsier, J-C. Peuzin, "Contactless actuationof bending and torsional vibrations for 2d-optical-scanner application," proc. Transducers '99, Sendai, Japan (1999), pp. 1876-1877.
3. Z.J. Yao, N.C. MacDonald, N.C. "Single crystal silicon supported thin film micromirrors for optical applications," Optical Engineering, 36 (no.5), pp. 1408-13 (1997).
4. J.-L.A Yeh, J. Hongrui; N.C. Tien, "Integrated polysilicon and DRIE bulk silicon micromachining for an electrostatic torsional actuator.", JMEMS, 8 (no.4), pp. 456-65 (1999)
5. H. Schenk, P. Durr, D. Kunze, H. Lakner, H. Kuck, "An electrostatically excited 2D-micro-scanning-mirror with an in-plane configuration of the driving electrodes," proc. MEMS 2000, Miyazaki, Japan (2000), pp. 473-478.
6. J. Hagerman, "Optimum spot size for raster-scanned monochrome CRT displays", Journal of the SID, 1 (no.3), pp. 367-369 (1993)
7. P.J. Brosen, "Dynamic Mirror Distortions in Optical Scanning," Applied Optics Vol. 11, No. 12, pp. 2987-2989, 1972.
8. D.J. Jacobs, Fundamentals of Optical Engineering, 1st ed. New York: McGraw-Hill, 1943.
9. W.P. Maszara, G. Goetz, A. Caviglia, and J.B. McKitterick, "Bonding of silicon wafers for silicon-on-insulator," Journal of Applied Physics, 64(10), pp. 4943-4950 (15 November 1988).
10. G.R. Elion, H.A. Elion, Electro-Optics Handbook, New York: Marcel Dekker, Inc., 1979.
11. M. Hart, R.A. Conant, K.Y. Lau, R.S. Muller, "Time-resolved measurement of optical MEMS, using stroboscopic interferometry," proc. Transducers '99, Sendai, Japan (June 1999), pp. 470-473.